Stable PbI_2-Terminated (001) Facets Drive Low-Defect Anisotropy for High-Performance Charge Transport in $MAPbI_3$ Single Crystals

Dong Liu[1†], Yuxin Li[1†], Dalin Li[1], Bin Lu[1], Zheng Guo[1], Qian Chen[1], Xiaojing Zhang[1], Yaxue Wang[1], and Tao He[1,2*]*

[1]State Key Laboratory of Crystal Materials, Shandong University, Jinan 250100, China

[2]Shenzhen Research Institute of Shandong University, Shenzhen 518057, China

E-mail: Dong Liu (ld1206@sdu.edu.cn) and Tao He (the@sdu.edu.cn).

† These authors contributed equally to this work.

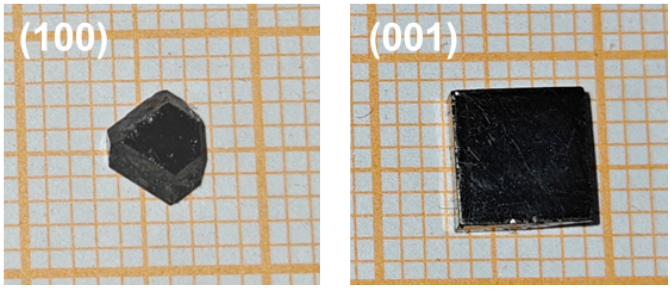

Fig. S1. Optical images of (100)- and (001)-oriented $MAPbI_3$ bulk single crystals.

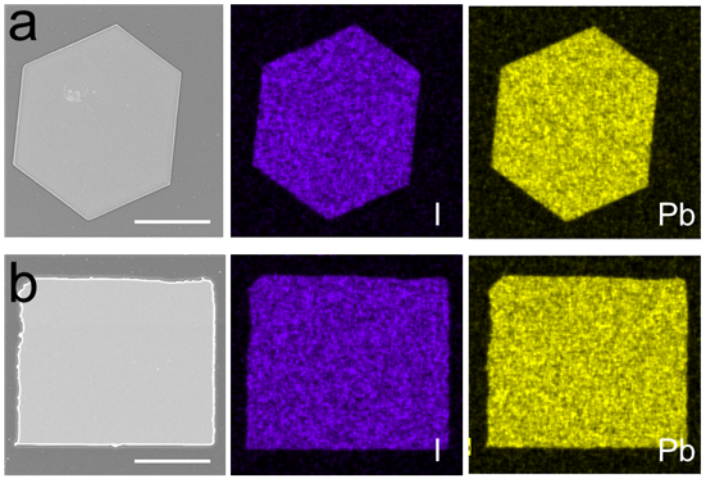

Fig. S2. SEM and EDS mapping of (a) $MAPbI_3$-(100) and (b) $MAPbI_3$-(001) facets. Scale bars are 20 μm.

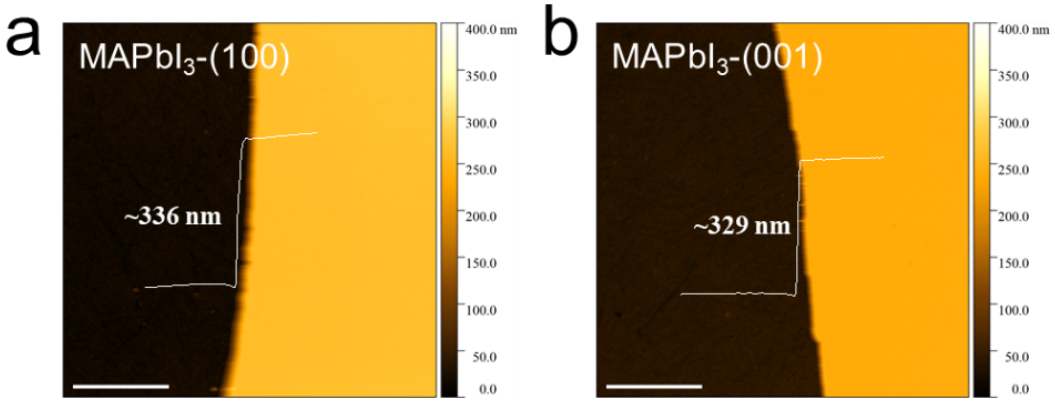

Fig. S3. AFM thickness measurements of the (a) $MAPbI_3$-(100) and (b) $MAPbI_3$-(001) facets.

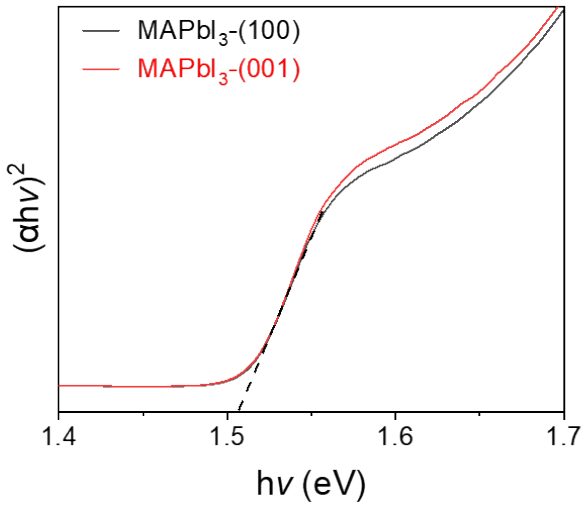

Fig. S4. Tauc plots of (100) and (001) facets of $MAPbI_3$ single crystals.

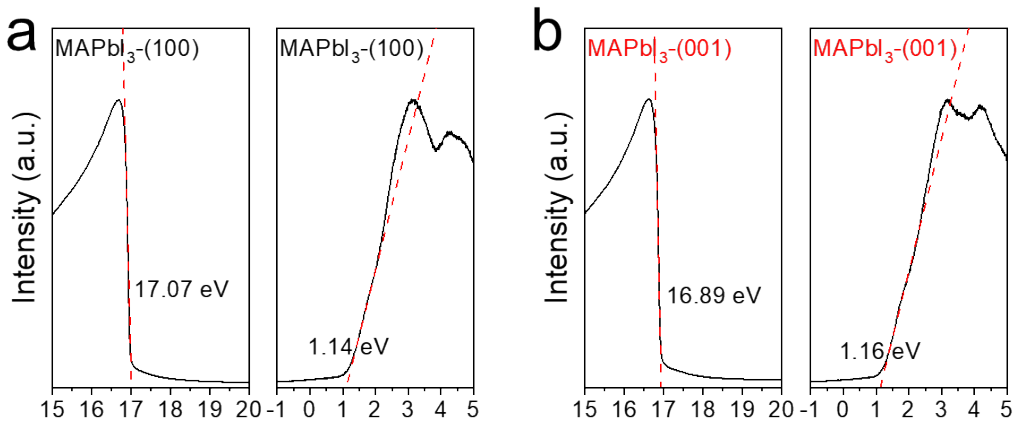

Fig. S5. UPS spectra of (a) $MAPbI_3$-(100) and (b) $MAPbI_3$-(001) facets.

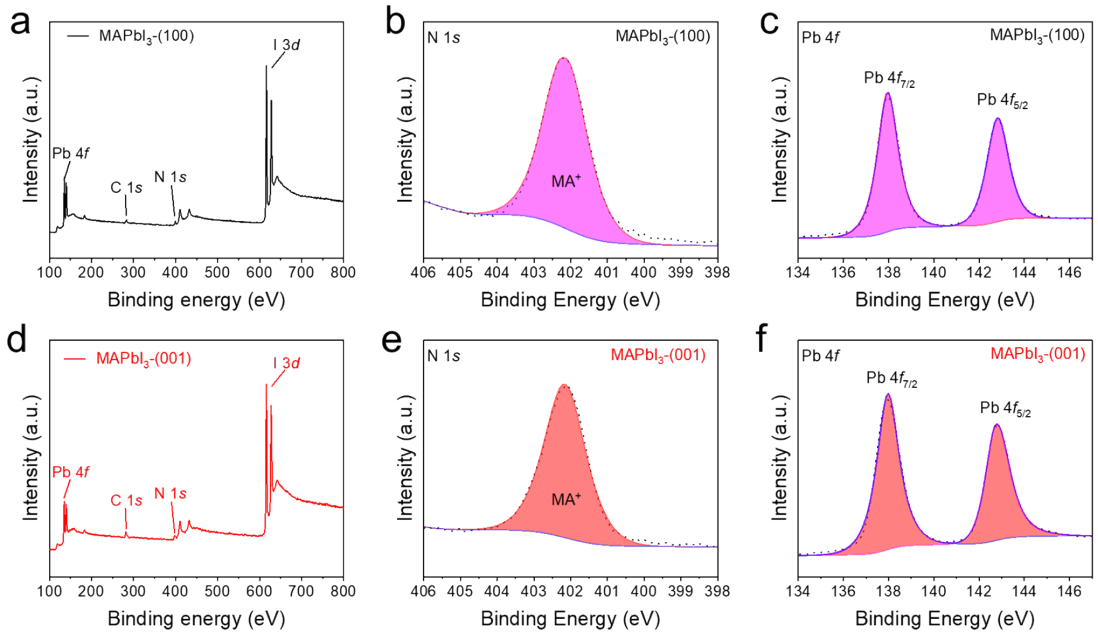

Fig. S6. (a–c) show the XPS survey scan, N 1*s*, and Pb 4*f* core-level spectra of the $MAPbI_3$-(100) facet, respectively. The corresponding spectra from the $MAPbI_3$-(001) facet are displayed in (d–f).

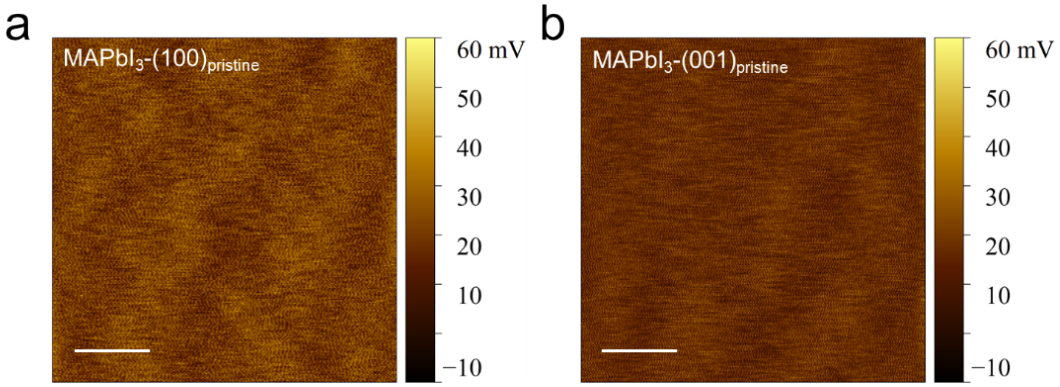

Fig. S7. Surface-potential images of the pristine (a) $MAPbI_3$-(100) and (b) $MAPbI_3$-(001) facets, respectively. The scale bar is 5 μm.

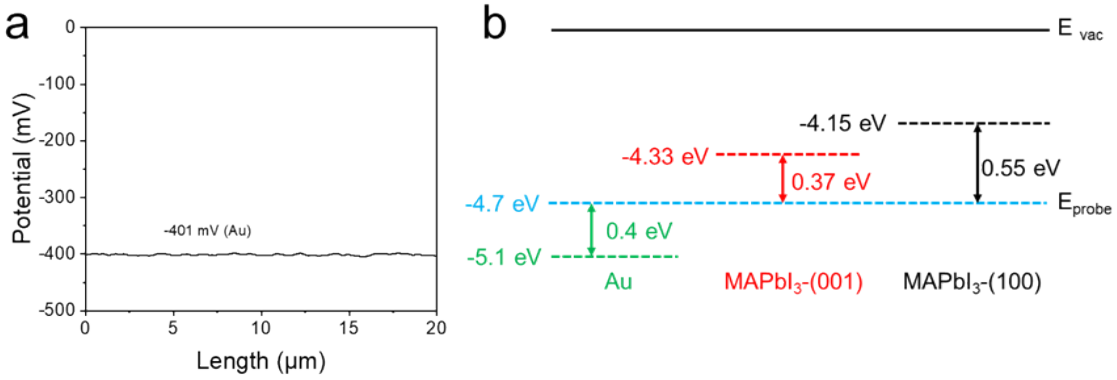

Fig. S8. Work function calibration of the KPFM probe. (a) Surface potential map of the 100 nm Au reference film on Si wafer. (b) Relative Fermi level alignment with respect to the vacuum level.

Prior to measurements, the probe work function was calibrated against a freshly evaporated Au reference (5.1 eV). The observed contact potential difference (CPD) of -401 mV yielded a calibrated probe work function of -4.7 eV. Post-calibration, CPD values of +550 mV (100) and +370 mV (001) were measured, corresponding to work functions of -4.15 eV and -4.33 eV, respectively.

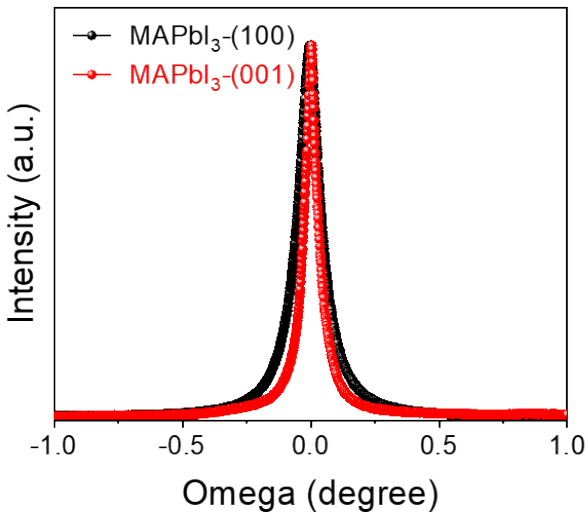

Fig. S9. XRD rocking curves of $MAPbI_3$-(100) and $MAPbI_3$-(001) facets.

Table S1. The full width at half-maximum (FWHM) of XRD rocking curves of $MAPbI_3$-(100) and $MAPbI_3$-(001) facets

Samples	FWHM of rocking curve (°)
$MAPbI_3$-(100)	0.158
$MAPbI_3$-(001)	0.103

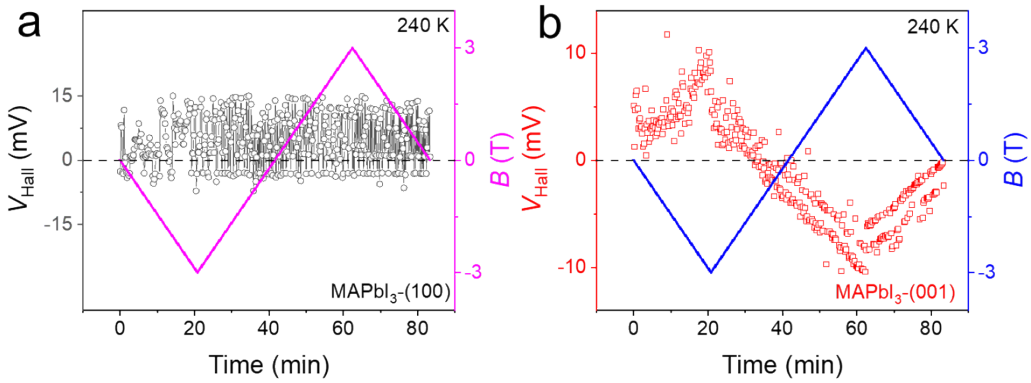

Fig. S10. Hall voltage measurements of (a) $MAPbI_3$-(100) and (b) $MAPbI_3$-(001) facets at 240 K. Hall measurements for the (100) facet at 240 K were precluded, presumably by ion migration.

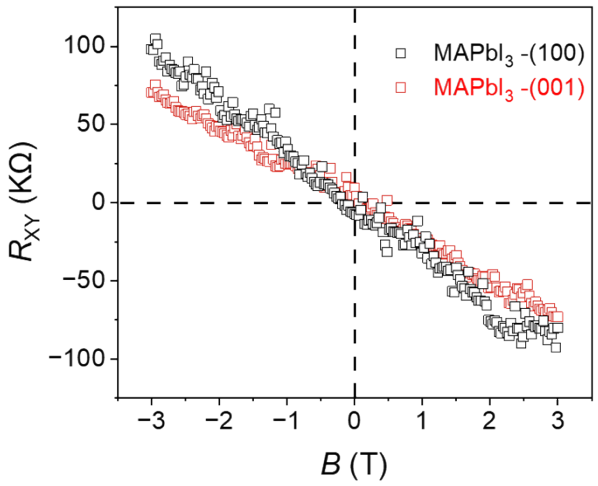

Fig. S11. Corresponding Hall resistance *Rxy* profile (180K) with respect to an external magnetic field *B*.

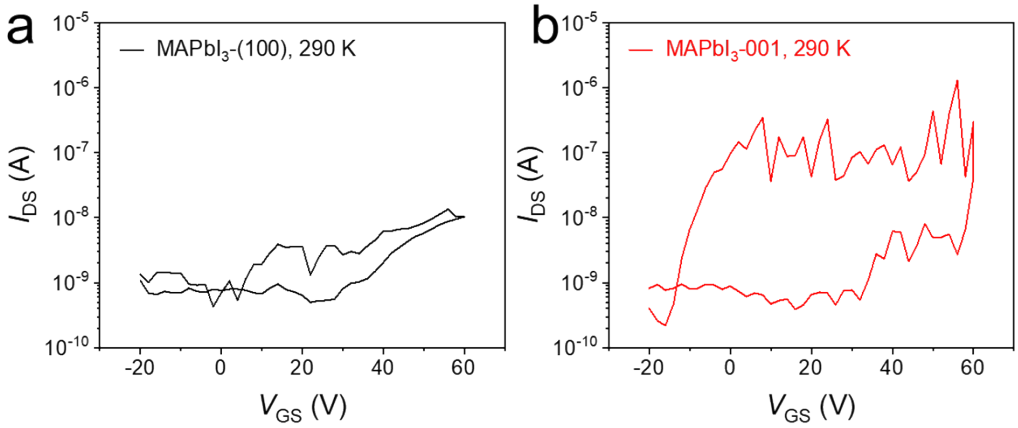

Fig. S12. Transfer characteristics of (a) $MAPbI_3$-(100) and (b) $MAPbI_3$-(001) facets measured at 290 K.

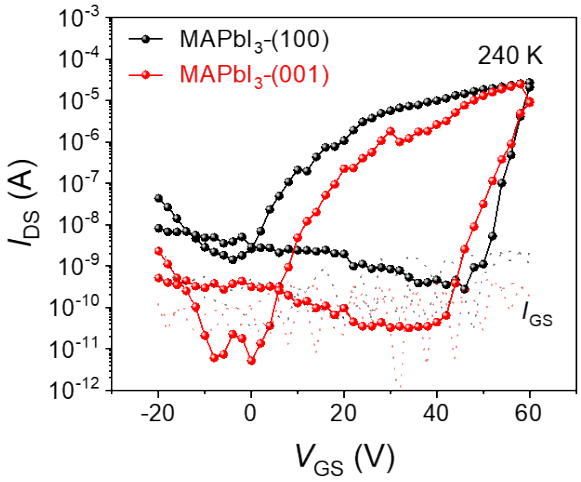

Fig. S13. Transfer characteristics of $MAPbI_3$-(100) and -(001) facets measured at 240 K.

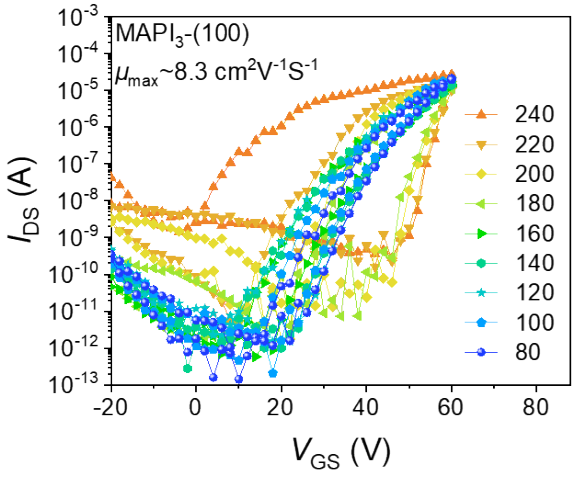

Fig. S14. Temperature dependent transfer curves of $MAPbI_3$-(100) facet.

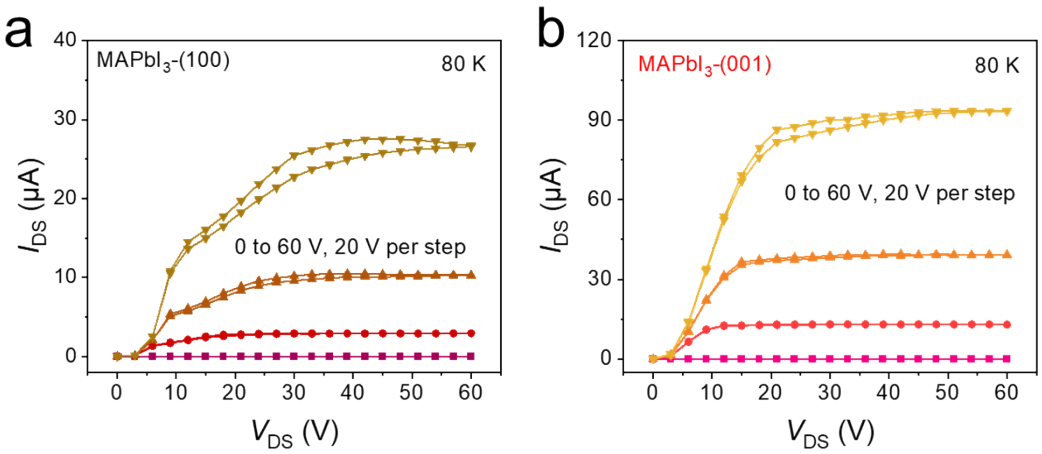

Fig. S15. Out characteristics of (a) $MAPbI_3$-(100) and (b) $MAPbI_3$-(001) facets measured at 80 K.

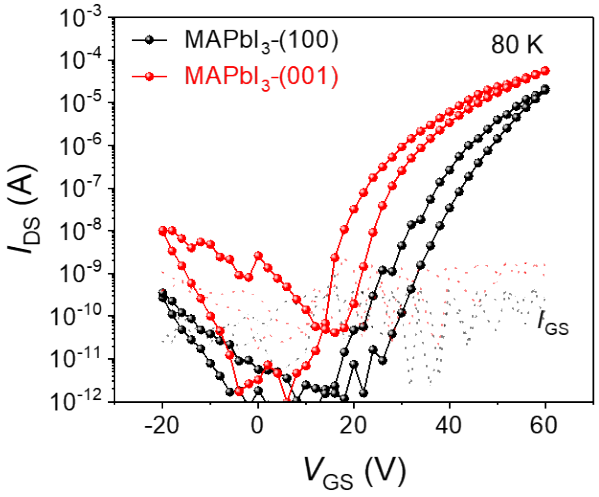

Fig. S16. Transfer characteristics of $MAPbI_3$-(100) and -(001) facets measured at 80 K.